

**Electronic structure, optical spectra, and x-ray magnetic circular dichroism in CoS<sub>2</sub>**V. N. Antonov,<sup>1,2</sup> O. V. Andryushchenko,<sup>1</sup> A. P. Shpak,<sup>1</sup> A. N. Yaresko,<sup>2</sup> and O. Jepsen<sup>2</sup><sup>1</sup>*Institute of Metal Physics, 36 Vernadsky Street, 03142 Kiev, Ukraine*<sup>2</sup>*Max-Planck-Institut für Festkörperforschung, Heisenbergstrasse 1, D-70569 Stuttgart, Germany*

(Received 28 April 2008; revised manuscript received 7 July 2008; published 10 September 2008)

The electronic structure, optical spectra, and x-ray magnetic circular dichroism (XMCD) of CoS<sub>2</sub> were investigated theoretically from first principles, using the fully relativistic Dirac linear muffin-tin orbital band-structure method. Densities of valence states, and orbital and spin magnetic moments are analyzed and discussed. The origin of the optical and XMCD spectra in the CoS<sub>2</sub> compound is examined. The band-by-band decomposition of the optical conductivity spectrum is presented and the interband transitions responsible for the prominent structures in the spectra are identified. The calculated results are compared with available experimental data.

DOI: [10.1103/PhysRevB.78.094409](https://doi.org/10.1103/PhysRevB.78.094409)

PACS number(s): 75.50.Cc, 71.20.Lp, 71.15.Rf

**I. INTRODUCTION**

Pyrite-type 3d transition-metal dichalcogenides  $MS_2$  ( $M = \text{Fe, Co, Ni, etc.}$ ) exhibit a wide variety of interesting electrical and magnetic properties.<sup>1</sup> The transition-metal 3d electron configuration varies from  $t_{2g}^6 e_g^0$  and  $t_{2g}^6 e_g^1$  to  $t_{2g}^6 e_g^2$  for FeS<sub>2</sub>, CoS<sub>2</sub>, and NiS<sub>2</sub>, respectively. FeS<sub>2</sub> is a semiconductor with a band gap of  $E_g \approx 0.9$  eV,<sup>2</sup> CoS<sub>2</sub> is metallic and orders ferromagnetically below  $T_c \approx 120$  K,<sup>3</sup> NiS<sub>2</sub> is an antiferromagnetic insulator with  $E_g \approx 0.3$  eV (Refs. 4 and 5), and  $T_N = 40$  K.<sup>6</sup> The transition-metal ions in these compounds are divalent and have a tendency to take low-spin states: FeS<sub>2</sub> is nonmagnetic ( $S=0$ ) and CoS<sub>2</sub> has a saturation moment of  $0.85\mu_B/\text{Co}$  (Ref. 3) close to that of  $S=1/2$ . NiS<sub>2</sub> is a high-spin ( $S=1$ ) compound.<sup>7</sup> NiSe<sub>2</sub> (Ref. 8) and CuS<sub>2</sub> (Ref. 9) are Pauli-paramagnetic metals.

CoS<sub>2</sub> has been considered as a candidate for a half-metallic ferromagnet (HMF), a metal for spin-up electrons and a semiconductor for spin-down electrons. The rapid development of magnetoelectronics intensified the interest in such materials. Adding the spin degree of freedom to the conventional electronic devices has several advantages such as nonvolatility, increased data processing speed, decreased electric power consumption, and increased integration densities.<sup>10,11</sup> The current advances in these materials are promising for engineering spintronic devices in the near future.<sup>11</sup>

CoS<sub>2</sub> has good lattice-constant matching with many semiconductors (GaAs, Si, ZnS, etc.) as reported by Kirczenow.<sup>12</sup> Despite extensive theoretical and experimental studies of CoS<sub>2</sub>,<sup>12–29</sup> its electronic and magnetic properties are not fully understood. Some of the experimental studies performed for CoS<sub>2</sub> are inconsistent with the theoretical prediction of a half-metallic character. Yamamoto *et al.*<sup>22</sup> observed significant reflectivity spectral changes at 120 K, and ascribed this temperature variation of reflectivity to the half metallicity of CoS<sub>2</sub>. However, the point-contact Andreev reflection measurement on the sulfur stoichiometric polycrystal<sup>27</sup> showed a relatively low-spin polarization of 56%, implying that CoS<sub>2</sub> is not half metallic. Polarized neutron-diffraction measurement on polycrystalline CoS<sub>2</sub> by Brown *et al.*<sup>28</sup> also showed that the half metallicity was not found in the ferromagnetic

phase. Recently Takahashi *et al.*<sup>26</sup> reported ultrahigh resolution ( $\Delta = 7$  meV) photoemission spectra (PES) on CoS<sub>2</sub> to study the temperature-induced change of the electronic structure across the Curie temperature. These PES results apparently disagree with the model of the electronic structure proposed by Yamamoto *et al.*<sup>22</sup> from the optical study. The PES clearly shows that the bottom of  $e_{g\downarrow}$  subband is located below  $E_F$  in the ferromagnetic phase while the optical study proposed a totally unoccupied  $e_{g\downarrow}$  subband located above  $E_F$ . The partially filled  $e_{g\downarrow}$  subband is consistent with the observed saturation magnetic moment of  $0.74\mu_B$ ,<sup>13</sup>  $0.85\mu_B$ ,<sup>30</sup> and  $0.87\mu_B$ ,<sup>27</sup> which requests a partially filled  $e_{g\downarrow}$  band in the ferromagnetic phase. A relatively small ( $\sim 58$  meV) Stoner-like excitation observed by inelastic neutron scattering<sup>20</sup> also favors the partially filled  $e_{g\downarrow}$  band. All these results show that a partially filled  $e_{g\downarrow}$  band plays an important role in characterizing the ferromagnetic property of CoS<sub>2</sub>.

The electronic structure calculations based on density-functional theory (DFT) show contradictory results for the half-metallic character of CoS<sub>2</sub>. Takahashi *et al.*,<sup>26</sup> using the full-potential linearized augmented plane-wave (FLAPW) method, obtained normal metallic ferromagnetic solution with partly occupied  $e_{g\downarrow}$  subband. Shishidou *et al.*<sup>25</sup> were able to obtain a half-metallic character of CoS<sub>2</sub> by using the FLAPW method combined with the generalized gradient approximation (GGA) (Ref. 31) for the exchange-correlation potential. Zhao *et al.*<sup>17</sup> and Kwon *et al.*<sup>24</sup> state that the CoS<sub>2</sub> is almost half metallic. Hobbs and Hafner<sup>23</sup> have studied the ground-state cohesive properties of CoS<sub>2</sub>, and obtained similar results using the projected augmented wave method. Kwon *et al.*<sup>24</sup> investigated the electronic structure of CoS<sub>2</sub> using the local spin-density approximation (LSDA) and taking into account the effect of the Coulomb correlation between Co 3d electrons by the LSDA+ $U$  method. The Coulomb correlation at Co sites was found to be relatively small,  $U \leq 1$  eV, and therefore CoS<sub>2</sub> may possibly be categorized as an itinerant ferromagnet. It was found that the observed electronic and magnetic behaviors of CoS<sub>2</sub> can be described better by the LSDA than by the LSDA+ $U$  method.

In the present study, we focus our attention on the optical properties and x-ray magnetic circular dichroism (XMCD) in the alloy CoS<sub>2</sub>. The optical spectra of CoS<sub>2</sub> have been investigated by several authors.<sup>5,16,22</sup> The x-ray magnetic circular

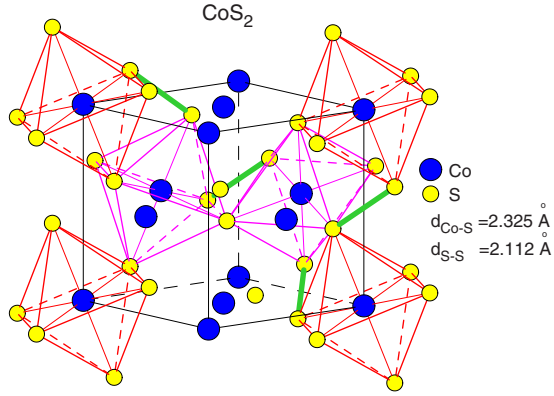


FIG. 1. (Color online) Schematic of the pyrite structure of  $\text{CoS}_2$  illustrating the linkage of the  $\text{CoS}_6$  octahedra. S-S dimers are marked by thick line.

dichroism in the ferromagnetic  $\text{CoS}_2$  alloy has been measured at the Co  $L_{2,3}$  and  $M_{2,3}$  edges by Miyauchi *et al.*,<sup>18</sup> and at the Co  $L_{2,3}$ ,  $M_{2,3}$ , and S  $L_{2,3}$  edges by Muro *et al.*<sup>19</sup> By analyzing the Co  $2p$  XMCD spectra with use sum rule, Muro *et al.*<sup>19</sup> evaluated  $\langle l_z \rangle / \langle s_z \rangle$  of Co as 0.18.

One should mention here that calculations based on DFT are not strictly applicable for excited-state properties, such as optical and XMCD spectra. DFT are developed to calculate the ground-state properties—magnetic moments, equilibrium volume, or bulk modules. Nevertheless, the electronic structure obtained from such calculations is often compared with optical, magneto-optical, or XMCD data, and good agreement between experiment and calculations is frequently observed.<sup>32</sup> In the limit of complete screening of the excited state, one would expect ground-state density-functional calculations to be able to describe the spectra well.

This paper is organized as follows. Section II presents a description of the  $\text{CoS}_2$  crystal structure and the computational details. Section III is devoted to the electronic structure, and optical and XMCD spectra of the  $\text{CoS}_2$  compound calculated in the fully relativistic Dirac linear muffin-tin orbital (LMTO) band-structure method. The calculated results are compared with the available experimental data. Finally, the results are summarized in Sec. IV.

## II. CRYSTAL STRUCTURE AND COMPUTATIONAL DETAILS

The schematic crystal structure for  $\text{CoS}_2$  is presented in Fig. 1. Due to its space group  $T_h^6 (Pa\bar{3}, \text{number } 205)$ , the cobalt atoms are located at the corners and the face centers of a cube, and eight S atoms are located at the positions of  $\pm(u, u, u; u + \frac{1}{2}, \frac{1}{2} - u, \bar{u}; \bar{u}, u + \frac{1}{2}, \frac{1}{2} - u; \frac{1}{2} - u, \bar{u}, u + \frac{1}{2})$ , in which  $u=0.389$  is a structural parameter.<sup>33</sup> The most important feature of the pyrite-type structure is that the nearest-neighbor S atoms interact covalently to form a S-S dimer (marked by thick green line in Fig. 1). Divalent  $\text{Co}^{2+}$  cations are located at the center of an octahedron comprised of  $\text{S}_2^{2-}$  anions. Each sulfur is shared by three different octahedra and a single dimer. The sulfur-cobalt interatomic distance in the octahedra is 2.325 Å while the sulfur-sulfur dimer S-S distance is 2.112 Å.

The details of the computational method are described in our previous papers,<sup>34,35</sup> and here we only mention some aspects specific to the present calculations. The calculations (corresponding to zero temperature) were performed for the experimentally observed lattice constant  $a=5.538$  Å using the spin-polarized fully relativistic (SPR) LMTO method.<sup>36,37</sup> We used the Perdew-Wang<sup>38</sup> parametrization for the exchange-correlation potential. Brillouin-zone (BZ) integrations were performed using the improved tetrahedron method<sup>39</sup> and charge self-consistently was obtained on a grid of 249  $\mathbf{k}$  points in the irreducible part of the BZ. To improve the potential we include additional empty spheres. The basis consisted of transition metal  $s$ ,  $p$ ,  $d$ ,  $f$ , and S  $s$ , and  $p$  and  $d$  LMTOs.

The absorptive part of the optical conductivity tensor was computed from the energy-band structure by means of the Kubo linear-response theory.<sup>40</sup> The dispersive part of the conductivity tensor is then obtained via the Kramers-Kronig transformation. To incorporate the intraband contribution to the optical conductivity tensor, we use the phenomenological Drude model<sup>41</sup> with intraband Drude relaxation time  $\gamma_D = 0.6$  eV. We mention that, furthermore, we have convoluted the calculated spectra with a Lorentzian whose width is 0.5 eV to approximate lifetime broadening.

In order to simplify the comparison between calculated and experimental x-ray absorption spectra (XAS), phenomenological background intensity was added to the calculated XAS. The background spectra are caused by different kinds of inelastic scattering of the electrons promoted to the conduction band above the Fermi level (scattering on potentials of surrounding atoms, defects, phonons, etc.). The problem is also well known in x-ray photoemission spectroscopy. The calculation of these processes from first principles is extremely difficult and has not been solved properly up to now. However, the background spectrum can be easily described phenomenologically.<sup>42,43</sup> In the present work the background intensity was approximated using a simple method describe in our previous paper.<sup>35</sup> A similar procedure was proposed by Röhler.<sup>44</sup>

It should also be mentioned that at photon energies far above the absorption edge the states with the next principal quantum number, e.g., Co  $4d$  states in the case of absorption at the Co  $L_{2,3}$  edge, contribute appreciably to the final-state wave function. As these states were not included into the LMTO basis set, the absorption intensity at high photon energies is underestimated in the calculations. The inclusion of the phenomenological background contribution compensates, at least to some extent, for this lack of the calculated XAS intensity.

Finally, the finite lifetime of a core hole was accounted for by folding the XMCD spectra with a Lorentzian. The widths of the  $K$ ,  $L_2$ , and  $L_3$  core-level spectra, with  $\Gamma_K=1.19$  eV,  $\Gamma_{L_2}=1.14$  eV, and  $\Gamma_{L_3}=0.41$  eV for Fe and  $\Gamma_K=0.52$  eV,  $\Gamma_{L_2}=0.09$  eV, and  $\Gamma_{L_3}=0.09$  eV for S, were taken from Ref. 45. The finite apparatus resolution of the spectrometer has been accounted for by a Gaussian of 0.6 eV.

## III. RESULTS AND DISCUSSION

### A. Energy band structure

The total and partial densities of states (DOSs) of  $\text{CoS}_2$  are presented in Fig. 2. The results agree well with previous

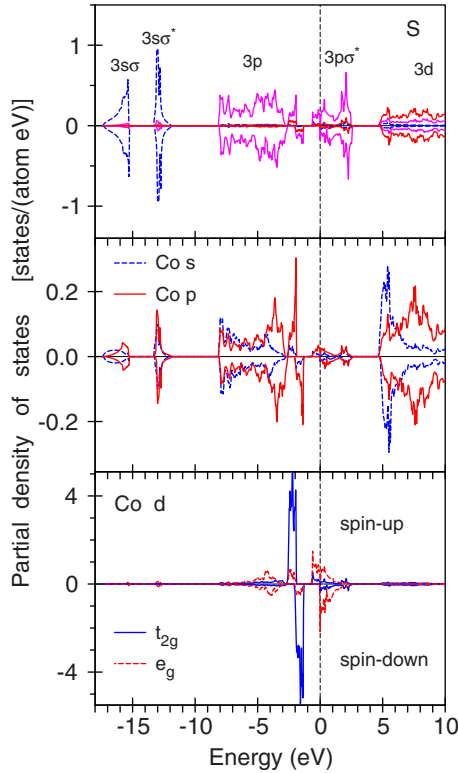


FIG. 2. (Color online) The partial [in states/(atom eV)] density of states of CoS<sub>2</sub>. The Fermi energy is at zero.

band-structure calculations.<sup>17,24,25</sup> The occupied part of the valence band can be subdivided into several regions. S  $3s$  states appear between  $-17.2$  and  $-11.8$  eV. Because of the strong covalent bonding nature of S-S dimers, each S band can be identified with corresponding molecular orbitals. The two peaks in the highest binding-energy side are the bonding S  $3s\sigma$  and the antibonding S  $3s\sigma^*$  bands, respectively.<sup>15,24</sup> The broadband of about 6.5 eV width between  $-8$  and  $-1.5$  eV consists mainly of S  $3p$ , which is a mixture of  $3p\sigma$ ,  $3p\pi$ , and  $3p\pi^*$  bands. The antibonding S  $3p\sigma^*$  intradimer band is located at 2.5 eV above the Fermi energy. S  $3d$  states are situated above 4.65 eV and separated from the antibonding S  $3p\sigma^*$  band by energy gap of 2.45 eV.

The crystal field at the Co site ( $S_6$  point symmetry) causes the  $d$  orbitals to split into a singlet  $a_g$ , and two doublets  $e_g'$  and  $e_g$ . The cubic component of the crystal field at the Co site is strong enough for the  $a_g$ ,  $e_g'$ , and  $e_g$  orbitals to form two separate nonoverlapping subbands. We present in Fig. 2 DOS of  $t_{2g}$  orbitals as a sum of the  $a_g$  and  $e_g'$  orbitals.

Co  $3d$  bands are formed in the energy range between S  $3p$  and S  $3p\sigma^*$  bands. Co  $t_{2g}$  bands are located between  $-1$  and  $-3$  eV below the Fermi energy  $E_F$  while the Co  $e_g$  bands cross  $E_F$ . The  $t_{2g}$  bands are nearly dispersionless with very narrow bandwidth, whereas the  $e_g$  bands near  $E_F$  are dispersive with a relatively large bandwidth of about 2.5 eV due to strong hybridization with the S  $3p\sigma^*$  band. The nearly half-metallic nature and the exchange splitting  $\Delta_{\text{ex}} \sim 1.0$  eV are prominent for the  $e_g$  band. CoS<sub>2</sub> is almost half metallic in the LSDA approximation. This feature is in agreement with that obtained by Zhao *et al.*,<sup>17</sup> Kwon *et al.*,<sup>24</sup> and Takahashi *et al.*<sup>26</sup> The electronic structure and the magnetism of CoS<sub>2</sub> are

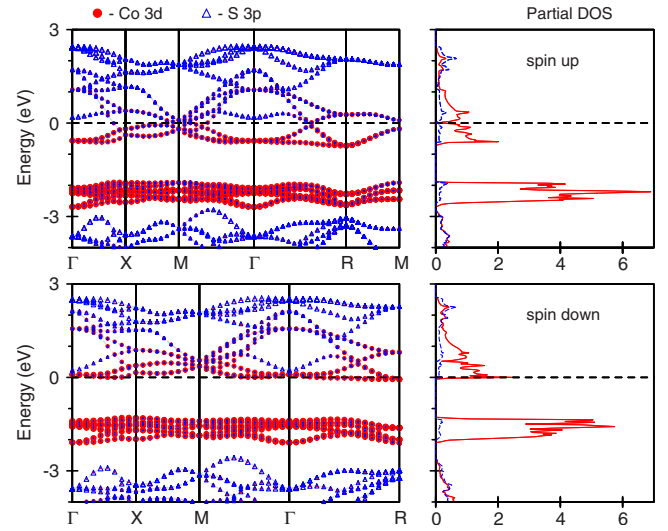


FIG. 3. (Color online) The energy-band dispersion in fat-band representation, and Co  $3d$  (red solid curve) and S  $3p$  (blue dashed curve) partial density of states [in states/(atom eV)] of CoS<sub>2</sub> calculated by the LSDA approximation.

closely related to the occupancy of the  $e_g$  states.

To show more clearly the degree of the Co  $3d$ -S  $3p$  hybridization, we present in Fig. 3 the energy-band structure of CoS<sub>2</sub> in fat-band representation. The size of the marker is proportional to the weight of the corresponding state in a Bloch wave function. The hybridization between the Co  $t_{2g}$  and S  $3p$  states is quite weak; however, as can be seen from the picture there is a strong hybridization between the Co  $e_g$  states and the S  $3p\sigma^*$  ones. Three energy bands in the 1.5–2.5 eV energy region above the Fermi level are predominantly of the S  $3p\sigma^*$  character. Although the energy bands between  $-0.7$  and 1.5 eV are mostly derived from the Co  $e_g$  states, the empty band closest to the Fermi energy is almost pure S  $3p$  band in the vicinity of the  $\Gamma$  symmetry point.

## B. Optical spectra

After the interpretation of the band structure above, we turn to the optical properties. In Fig. 4 the experimental<sup>16</sup> imaginary part of the dielectric function  $\epsilon_{2,\text{xx}}$ , and the optical reflectivity and imaginary part of the energy-loss function  $\text{Im}[-1/\epsilon(\omega)]$  of CoS<sub>2</sub> are compared with the theoretically calculated spectra within the LSDA approach in a wide energy range.

The experimental features of the optical functions are reasonably well reproduced in the LSDA calculations except for the energy shift toward smaller energies of the prominent peak in the theoretically calculated energy-loss function. One of the possible reasons for this is the use in our calculations of the linear band-structure method LMTO with a fixed set of linearization energies ( $E_\nu$ ), which can produce a shift in the energy-band position for the high energy interval (over 20 eV). The theoretically calculated optical reflectivity spectrum of CoS<sub>2</sub> is larger than the experimental measurements. One of the possible reasons for this is a nonideal sample surface, in which roughness can reduce the optical reflectivity.

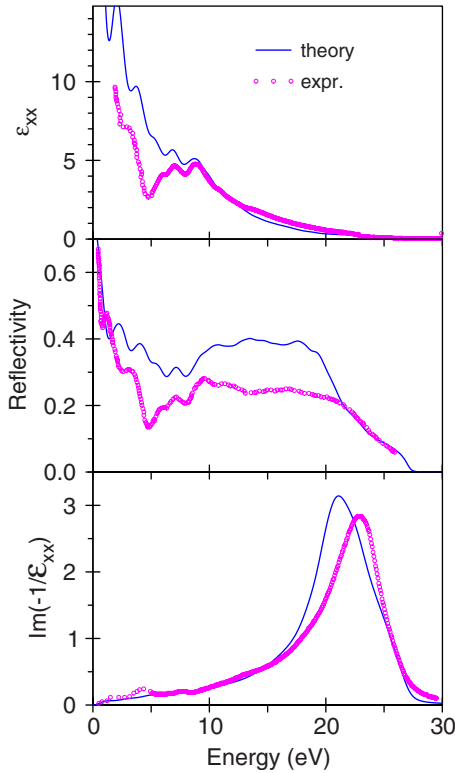


FIG. 4. (Color online) The diagonal part of the dielectric function  $\epsilon_{xx}$ , optical reflectivity, and energy-loss spectrum of CoS<sub>2</sub> calculated in the LSDA approximation compared with the experimental data (Ref. 16) (open circles).

To explain the microscopic origin of the optical properties of CoS<sub>2</sub> in terms of individual electronic transitions, we decomposed the calculated  $\sigma_{1,xx}$  spectrum into the contributions arising from separate interband transitions. This can be done because the corresponding bands are well separated in energy. As one may see in Fig. 5, the first peak A situated at 0.5 eV originates completely from the Co  $e_{g\uparrow} \rightarrow e_{g\uparrow}$  interband transitions. To avoid misunderstanding, we should mention that here and in the following, when talking about  $d \rightarrow d(p \rightarrow p)$  transitions, we mean that the energy bands involved in the transitions have predominantly  $d(p)$  character. However, the contribution of  $p(d)$  states to these bands is sufficient to provide a significant transition probability through optical dipole matrix elements. The next feature B at 2.2 eV comes from the Co  $t_{2g\uparrow} \rightarrow e_{g\uparrow}$ , the Co  $t_{2g\downarrow} \rightarrow e_{g\downarrow}$ , and the Co  $e_{g\uparrow} \rightarrow S p\uparrow$  interband transitions. The peak C arises from the  $S p \rightarrow e_g$  and Co  $t_{2g} \rightarrow S 3p\sigma^*$  in both the spin-up and spin-down channels. The peak D is mostly derived from the  $S p \rightarrow S p$  and also Co  $t_{2g} \rightarrow (S 3d, Co 4s, Co 4p)$  interband transitions. The high energy peak F is from the  $S p \rightarrow (S 3d, Co 4s, Co 4p)$  transitions. In real optical experiments interband transitions are obscured by broadening from intraband Drude-like transitions and lifetime effects.

The largest discrepancy between the theoretically calculated and experimentally measured spectra occurs at the 0–5 eV energy range. Figure 6 presents the theoretically calculated and experimental<sup>22</sup> optical reflectivity, and theoretical conductivity spectra in this energy interval. Overall, the spectral shape of the experimental optical reflectivity spec-

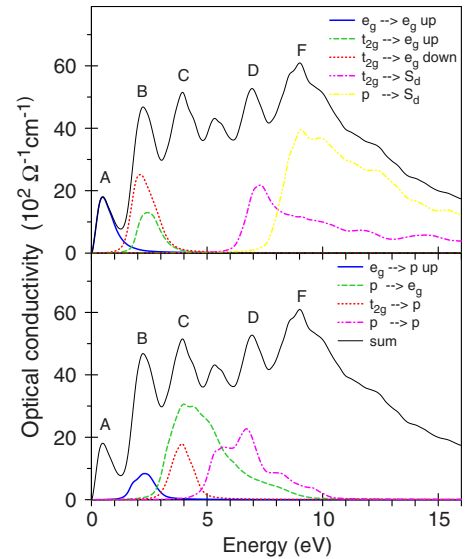


FIG. 5. (Color online) The decomposition of the absorptive part of the diagonal optical conductivity  $\sigma_{xx}^1$  of CoS<sub>2</sub> into partial interband transitions;  $p$  stands for S 3*p*, and  $e_g$  and  $t_{2g}$  are Co orbitals. The origin of the peaks A–F is discussed in the text.

trum is qualitatively reproduced by the LSDA calculations. However, the positions of the calculated prominent peaks of the optical reflectivity, which correspond to the peaks A, B, and C in optical conductivity spectrum, are shifted toward higher energies as compared to the experiment.

The positions of the peaks A, B, and C are sensitive to the bonding-antibonding splitting of the  $p\sigma$  states of S-S dimers, and to the crystal-field splitting between Co  $t_{2g}$  and  $e_g$  bands, which can be illustrated by varying the value of the internal structural parameter  $u$  or the lattice constant. With the de-

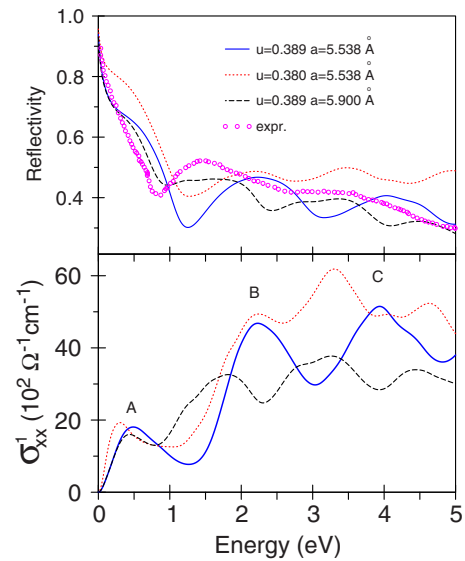


FIG. 6. (Color online) Contributions of different interband transitions to the absorptive part of the diagonal optical conductivity, and optical reflectivity spectrum of CoS<sub>2</sub> calculated for different structure parameters  $u$  in comparison with the experimental measurements (Ref. 22) (open circles). Peaks A–C correspond to those in Fig. 5

crease in  $u$ , the S-S separation within a dimer increases, which results in reduction in the  $p\sigma$  bonding-antibonding splitting. The Co-S distance in a  $\text{CoS}_6$  octahedron also increases but to lesser extent so that the  $t_{2g}-e_g$  splitting is almost unaffected by the variation of  $u$ . The increase in the lattice constant, on the other hand, leads to strong decrease in the  $t_{2g}-e_g$  splitting, which is determined by the strength of the Co  $d-S p$  hybridization.

The coupling of the structural parameter  $u$  to magnetic order and band structure was observed earlier.<sup>46,47</sup> It should be noticed that the parameter  $u$  in pyrite-type  $3d$  transition-metal dichalcogenides varies in quite a wide range according to different experimental measurements ( $\Delta u=0.007$  and  $0.008$  for  $\text{FeS}_2$  and  $\text{CoS}_2$ , respectively). We found that the dimer S-S distance increases from  $2.113 \text{ \AA}$  for the experimental  $u=0.389$  to  $2.302 \text{ \AA}$  for the  $u=0.380$  in  $\text{CoS}_2$ .

Decreasing  $u$  from  $0.389$  to  $0.380$  leads to the shift of the peak  $C$  in  $\sigma_{1xx}$  toward lower energy by  $0.7 \text{ eV}$  and improves the agreement with the experiment in the position of the corresponding peak of the optical reflectivity spectrum (Fig. 6). Similar conclusion was made by Wu *et al.*<sup>47</sup> They used angle-resolved and energy-dependent photoemissions from high-quality single-crystal samples to study the band structure of the  $\text{CoS}_2$ . The experimental data suggest the presence of at least one Fermi-level crossing along the  $\Gamma-X$  line, which is absent either in LSDA or in GGA, and is unlikely to appear if correlations were included. They therefore suggest that the disagreement with the experiment may be due to a slight error in the S-S bonding-antibonding splitting. It was shown that the sulfur bands notably shift down when the S-S separation is increased, and for the decreased value in  $u=0.387$  they cross the Fermi level in both spin channels. It was suggested that the half-metallic gap in  $\text{CoS}_2$  may be controlled by the bonding-antibonding splitting in this dimer rather than by exchange splitting on the Co atoms.

As can be seen from Fig. 6 the decrease in the  $u$  value indeed improves the energy position of the peak  $C$ . However, the positions of the peaks  $A$  and  $B$  did not change. The latter two peaks arise from the interband transitions between the Co  $3d$  bands (see Fig. 5). Therefore LSDA calculations produce incorrect relative energy positions of Co  $t_{2g}$  and  $e_g$  bands. Recent angle-integrated PES measurements of  $\text{CoS}_2$  by Takahashi *et al.*<sup>26</sup> with He  $I\alpha$  ( $21.218 \text{ eV}$ ) and He  $II\alpha$  ( $40.814 \text{ eV}$ ) photons place the Co  $t_{2g}$  states at around  $1 \text{ eV}$  binding energy while the Co  $e_g$  states are found in close vicinity of the Fermi energy. In our LSDA calculations, the Co  $t_{2g}$  states lie at  $1.9 \text{ eV}$  below the Fermi energy, similar to the results obtained by the FLAPW method.<sup>26</sup>

Figure 6 shows the theoretically calculated optical reflectivity spectrum for reduced lattice constant of  $a=5.9 \text{ \AA}$ . The occupied Co  $t_{2g}$  states became narrower for this lattice constant and shift upward by  $0.8 \text{ eV}$ . The Co  $e_g$  states are changed to lesser extent. As can be seen from Fig. 6 the increased value in lattice parameter leads to energy shift of the peaks  $B$  and  $C$  toward smaller energy, in better agreement with the optical reflectivity experiment. The energy position of the Co  $t_{2g}$  states for reduced lattice constant  $a=5.9 \text{ \AA}$  is equal to  $-1.1 \text{ eV}$ , in good agreement with the PES measurements.<sup>26</sup>

One of the possible reasons for the observed discrepancy between the optical and PES measurements, and the LSDA

calculations might be nonexact treatment of the electron exchange and correlations. One should mention that, although the self-energy correction frequently improves the agreement between theory and experiment, the renormalization of quasiparticle energies mostly affect the widths of the energy bands.<sup>48</sup> In our particular case the LSDA approximation fails to produce correct relative Co  $t_{2g}-e_g$  energy-band split, which is determined by the strength of the nearly octahedral  $S_6$  environment. With the increase in the lattice constant  $S$  atoms move further away from Co, which reduces the Co  $3d-S 3p$  hybridization strength and, therefore, the Co  $t_{2g}-e_g$  splitting.

For better understanding of the electronic structure of  $\text{CoS}_2$ , the correlation effects should be appropriately included in the theoretical model and these corrections should also affect the Co  $3d-S 3p$  hybridization strength.

The present band-structure calculations disagree with the model of electronic structure proposed from the optical study by Yamamoto *et al.*<sup>22</sup> in two points: the position of  $e_{g\downarrow}$  subband and splitting of  $t_{2g}$  states in the ferromagnetic phase. As clearly seen in Figs. 2 and 3, the bottom of  $e_{g\downarrow}$  subband is located below  $E_F$  in the ferromagnetic phase while the model based on the optical study proposed a totally unoccupied  $e_{g\downarrow}$  subband located above  $E_F$ . A non-half-metallic ferromagnetic state is consistent with the observed saturation magnetic moment of  $0.85 \mu_B$ .<sup>30</sup> A relatively small ( $\sim 58 \text{ meV}$ ) Stoner-like excitation observed by inelastic neutron scattering<sup>20</sup> also favors the partially filled  $e_{g\downarrow}$  band. Finally the partially filled  $e_{g\downarrow}$  subband is well reproduced by the PES measurements by Takahashi *et al.*<sup>26</sup>

The optical study also proposed that the  $t_{2g}$  states should split into two subbands with up and down spins, respectively, in the ferromagnetic phase. However, from our LSDA calculations, we found quite small exchange splitting of the  $t_{2g}$  states (Fig. 2). As clearly seen in Fig. 5 interband transitions  $t_{2g} \rightarrow e_{g\uparrow}$  and  $t_{2g} \rightarrow e_{g\downarrow}$  occupy the same energy interval. It is inconsistent with the resonant photoemission results,<sup>49</sup> which indicate that the  $t_{2g}$  bands do not show any temperature-induced change even across  $T_C$ .

### C. X-ray magnetic circular dichroism spectra

The x-ray magnetic circular dichroism in the ferromagnetic  $\text{CoS}_2$  alloy has been measured at the Co  $L_{2,3}$  and  $M_{2,3}$  edges by Miyauchi *et al.*,<sup>18</sup> and at the Co  $L_{2,3}$ ,  $M_{2,3}$ , and  $S L_{2,3}$  edges by Muro *et al.*<sup>19</sup>

#### 1. Co $L_{2,3}$ x-ray magnetic circular dichroism spectra

Figure 7 shows the calculated isotropic x-ray absorption and XMCD spectra of Co at the  $L_{2,3}$  edges in the LSDA approach together with the experimental data.<sup>19</sup> The contribution from the background scattering is shown by dotted line in the upper panel of Fig. 7.

The experimental Co XAS has a pronounced shoulder at the  $L_3$  peak shifted by about  $4-8 \text{ eV}$  with respect to the maximum of higher photon energy. This feature is due to the transitions from  $2p$  core level to empty Co  $4s$  states separated from the antibonding  $S 3p\sigma^*$  and Co  $e_g$  bands by an energy gap (see Fig. 2). This structure is less pronounced at

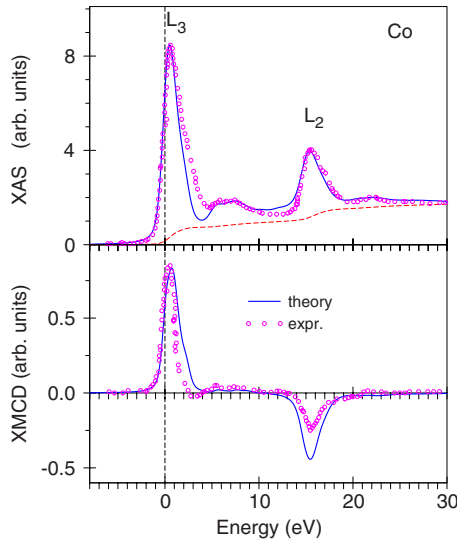


FIG. 7. (Color online) Upper panel: x-ray absorption spectra of  $\text{CoS}_2$  at the Co  $L_{2,3}$  edges calculated in the LSDA approximation (full line) and experiment (Ref. 19) (circles). Experimental spectra were measured with an external magnetic field of 1.1 T. Dotted line shows the theoretically calculated background spectrum. Lower panel: theoretically calculated (full line) and experimental (Ref. 19) (circles) XMCD spectra of  $\text{CoS}_2$  at the Co  $L_{2,3}$  edges.

the  $L_2$  edge, which can be ascribed to the lifetime broadening effect. The lifetime of the  $2p_{1/2}$  core hole is shorter than the  $2p_{3/2}$  core hole due to the  $L_2L_3V$  Coster-Kronig decay.

The XMCD spectra at the  $L_{2,3}$  edges are mostly determined by the strength of the spin-orbit coupling of the initial  $2p$  core states and spin polarization of the final empty  $3d_{3/2,5/2}$  states. Moreover, the exchange splitting of the  $2p$  core states as well as the SO coupling of the  $3d$  valence states are of minor importance for the XMCD at the  $L_{2,3}$  edge of  $3d$  transition metals.<sup>32</sup> The LSDA calculations reproduce the experimental Co  $L_{2,3}$  XMCD spectra very well although the calculated magnetic dichroism is somewhat too high at the  $L_2$  edge in comparison with the experiment.

In magnets, the atomic spin  $M_s$  and orbital  $M_l$  magnetic moments are basic quantities, and their separate determination is therefore important. Our LSDA calculations produce a local spin and orbital magnetic moments of  $0.734\mu_B$  and  $0.032\mu_B$  on a Co site with  $M_l/M_s=0.044$ , i.e.,  $\langle l_z \rangle / \langle s_z \rangle = 0.088$ . The sulfur spin moment is equal to  $0.043\mu_B$ , whereas the calculated S orbital moment is vanishingly small.

Using the magneto-optic sum rules for the Co  $L_{2,3}$  spectra, the orbital magnetic moment at the Co site was estimated as  $0.06\mu_B$  with the  $\langle l_z \rangle / \langle s_z \rangle$  ratio of 0.18.<sup>19</sup> These results were obtained by neglecting the magnetic-dipole moment  $T_z$ , and the overlap between the  $2p_{3/2}$  and  $2p_{1/2}$  absorption bands.

The value of the Co orbital magnetic moments derived from the experimental XMCD spectra is considerably higher in comparison with our band-structure calculations. There are two possible sources for the discrepancy between the theory and the experiment.

It is a well-known fact that LSDA calculations are inaccurate in describing orbital magnetism.<sup>32,50</sup> In the LSDA, the

Kohn-Sham equation is described by a local potential that depends on the electron-spin density. The orbital current, which is responsible for  $M_l$ , is, however, not included in the equations. This means that, although  $M_s$  is self-consistently determined in the LSDA, there is no framework to determine simultaneously  $M_l$  self-consistently. To calculate  $M_l$  beyond the LSDA scheme, we used the rotationally invariant LSDA+ $U$  method.<sup>51</sup> We used  $U=J=0.89$  eV for the transition-metal sites. In this case  $U_{\text{eff}}=U-J=0$  and the effect of the LSDA+ $U$  comes from nonspherical terms, which are determined by  $F^2$  and  $F^4$  Slater integrals. This approach is similar to the orbital polarization (OP) correction derived by Brooks and co-workers,<sup>52–54</sup> and Mavromaras *et al.*<sup>55</sup> The LSDA+OP calculations produce orbital magnetic moments equal to  $0.052\mu_B$  with  $M_l/M_s=0.065$  ( $\langle l_z \rangle / \langle s_z \rangle = 0.13$ ), in good agreement with the experimental data.<sup>19</sup>

On the other hand, it is well known that the XMCD sum rules are derived within an ionic model using a number of approximations.<sup>50</sup> It is interesting to compare the spin and orbital moments obtained by applying the sum rules to the theoretically calculated XAS and XMCD spectra with the directly calculated LSDA values. We found that the sum rules reproduce the spin and orbital magnetic moments within 44% and 62%, respectively. The largest error comes from the energy dependence of the radial matrix elements.<sup>35</sup> We applied the sum rules to the theoretically calculated XMCD spectra, neglecting the energy dependence of the radial matrix elements. This approximation reduces the disagreement in spin magnetic moments to 9% and, in the orbital moment, to 8%. These results show that the energy dependence of the matrix elements may strongly affect the values of the spin and orbital magnetic moments derived by applying the sum rules to experimental XMCD spectra.

## 2. Co $M_{2,3}$ x-ray magnetic circular dichroism spectra

Figure 8 shows the calculated isotropic x-ray absorption and XMCD spectra of Co at the  $M_{2,3}$  edges in the LSDA approach together with the experimental data.<sup>18,19</sup> As observed in Fig. 8, the Co  $3p_{3/2}$  and  $3p_{1/2}$  absorption spectra are mixed because of the small spin-orbit splitting. Therefore, the analysis of the XMCD spectrum is rather difficult in this region. An intensive structure is observed in the energy region just below the absorption edge in the experimental XAS, which is not reproduced theoretically. This structure is caused by the Fano effect due to an interference between the direct photoemission from the  $3d$  state and the super Coster-Kronig decay following the  $3p \rightarrow 3d$  core excitation.<sup>19</sup> Such complicated process is not included theoretically in this study.

The Co  $M_{2,3}$  XMCD spectra, besides the preedge structure, consist of two major peaks. The positive peak at around 1 eV is formed by the  $M_3$  spectrum and the higher energy negative peak at 3.5 eV corresponds mostly to the  $M_2$  one. There is additionally a small positive structure at 5 eV in Ref. 19 and at 6.5 eV in Ref. 18. This structure is less pronounced in the theoretically calculated spectrum.

## 3. S $L_{2,3}$ x-ray magnetic circular dichroism spectra

Figure 9 presents the calculated XAS as well as XMCD spectra of the  $\text{CoS}_2$  alloy at the S  $L_{2,3}$  edges compared with

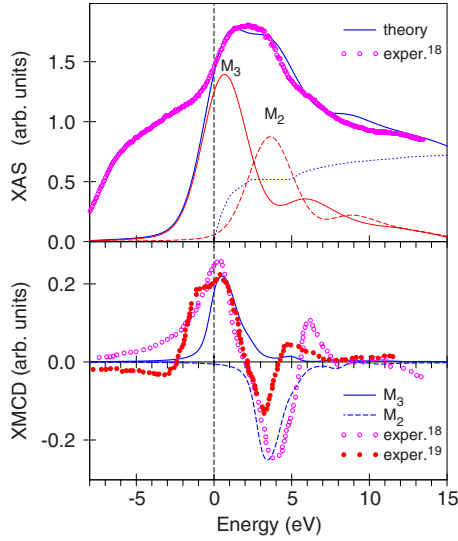


FIG. 8. (Color online) Upper panel: experimental (Ref. 18) (circles) x-ray absorption spectra of CoS<sub>2</sub> at the Co  $M_{2,3}$  edges and calculated spectra in the LSDA approximation (thin full line for the  $M_3$  edge and dashed thin line for the  $M_2$  one). Dotted line shows the theoretically calculated background spectra; full thick line is the sum of the theoretical XAS and background spectra. Lower panel: theoretically calculated XMCD spectra at the  $M_3$  (full line) and  $M_2$  (dotted line) in comparison with the experimental spectra of Refs. 18 (open circles) and 19 (full circles).

the experimental data.<sup>19</sup> The SO splitting of S  $2p$  level is even smaller compared with the Co  $3p$  one; therefore the S  $2p_{3/2}$  and  $2p_{1/2}$  absorption and XMCD spectra strongly overlap. We display in Fig. 9 the XAS and XMCD spectra as a sum of the  $L_3$  and  $L_2$  ones.

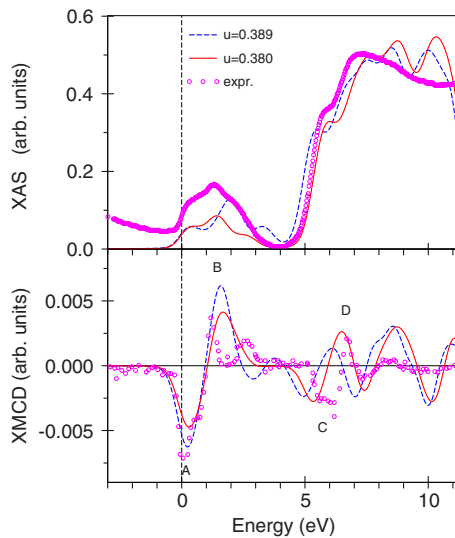


FIG. 9. (Color online) Upper panel: experimental (Ref. 19) (circles) x-ray absorption spectra of CoS<sub>2</sub> at the S  $L_{2,3}$  edges and calculated spectra in the LSDA approximation for different structural parameters  $u$  (dotted line for  $u=0.389$  and full line for  $u=0.380$ ). Lower panel: theoretically calculated XMCD spectra at the S  $L_{2,3}$  edges for different structural parameters  $u$  in comparison with the experimental spectra (Ref. 19) (open circles).

The experimentally measured S  $L_{2,3}$  x-ray absorption spectrum consists of two peaks separated by an energy gap. This reflects the energy distribution of the corresponding S partial DOSs (see Fig. 2). The first fine structure closer to the edge is formed by the transitions to the  $3p\sigma^*$  states while the more intensive structure above 4.5 eV is due to S  $2p \rightarrow 3d$  interband transitions. There is a small disagreement in the energy position of the fine structures in both the low and high energy peaks. Similarly to the case of the optical spectra, we suggest that the disagreement with the experiment may be due to a slight error in the S-S bonding-antibonding splitting. To illustrate the consequences of this possible error, the internal structural parameter  $u$  was varied in order to understand its effect on the XAS and XMCD spectra. We found that decreasing  $u$  from 0.389 to 0.380 leads to the shift of the S  $3p$  and  $3d$  partial DOSs toward lower energy, and improves the agreement with the experiment in the position of fine structures of the x-ray absorption spectrum (Fig. 9). The decreased value in  $u$  also improves slightly the energy position of peaks C and D in the XMCD spectra. One should mention that the reduced value in the lattice constant  $a = 5.9 \text{ \AA}$ , which improves the Co  $t_{2g} - e_g$  splitting almost does not affect the shape of the XAS and XMCD spectra, which reflect the energy distribution of empty energy states.

For the energies higher than 8 eV, the theory shows some additional oscillating structures while the experimental spectrum is a smooth function of energy. The oscillatory behavior of the high energy part of the theoretical spectrum above 8 eV may possibly be damped by the quasiparticle lifetime effects, which is not taken into account in our calculations.

#### 4. Co and S x-ray magnetic circular dichroism spectra at the K edge

The x-ray absorption and XMCD spectra in metals at the K edge in which the  $1s$  core electrons are excited to the  $p$  states through the dipolar transition usually attract only minor interest because  $p$  states are not the states influencing magnetic or orbital order. Recently, however, understanding  $p$  states has become important since XMCD spectroscopy using K edges of transition metals became popular. The K edge XMCD is sensitive to the electronic states at neighboring sites because of the delocalized nature of the  $p$  states. It is documented that sizable XMCD signals can be detected at the K edge of nonmagnetic atoms such as sulfur, oxygen, and nitrogen in ferromagnetic EuS,<sup>56</sup> EuO,<sup>57</sup> and GdN.<sup>58,59</sup>

There are no experimental measurements of the XAS and XMCD spectra at the Co and S K edges of CoS<sub>2</sub>; therefore we present only the theoretically calculated spectra in Fig. 10. The main x-ray absorption in Co XAS occurs above 4 eV with relatively low intensity in 0–4 eV energy range above the K edge. The most intense x-ray absorption in S K XAS is at low energy less than 4 eV because the absorption in this energy range is due to the S  $1s \rightarrow 3p\sigma^*$  interband transitions.

The S  $3p$ –Co  $3d$  hybridization and the spin-orbit interaction in the  $3p$  states play crucial roles for the S K edge dichroism. The K XMCD spectra originates in the orbital polarization of the empty  $p$  states, which may be induced (1) by the spin polarization of the  $p$  states through the spin-orbit interaction and (2) by the orbital polarization at neighboring

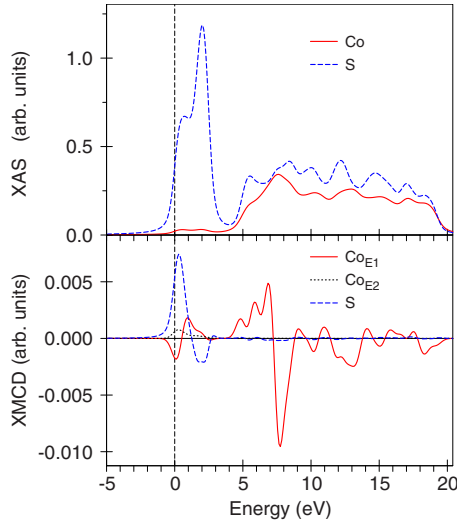


FIG. 10. (Color online) Upper panel: theoretically calculated x-ray absorption spectra of  $\text{CoS}_2$  at the Co (full line) and S (dashed line)  $K$  edges. Lower panel: theoretically calculated XMCD spectrum at the S  $K$  (dashed line) and Co  $K$  edges, taking into account only dipole allowed  $E_1$  transitions (full line) and only quadrupole  $s \rightarrow d$  transitions (dotted line). Dichroic signal at the Co  $K$  edge is multiplied by factor of ten.

sites through hybridization. We calculated the  $K$  XMCD spectrum at the S site with the spin-orbit interaction (SOI) turned off separately for the S  $3p$  and the Co  $3d$  states. We found that the  $K$  XMCD spectrum changes slightly when the SOI on the S site is turned off while the spectrum almost disappears (reduced its intensity almost two orders of magnitude) when the SOI on the Co site is turned off. This indicates that the SOI on Co site influences the orbital mixture of S  $3p$  states through the S  $3p$ –Co  $3d$  hybridization. It is important to note that the S  $K$  dichroic signal is expected to be one order of magnitude larger than at the S  $K$  edge in  $\text{CoS}_2$ .

We investigated also the effect of the electric quadrupole  $E_2$  and magnetic-dipole  $M_1$  transitions for the Co  $K$  XAS and XMCD spectra. We found that the  $M_1$  transitions are extremely small in comparison with the  $E_2$  transitions and can be neglected. The  $E_2$  transitions are much weaker than electric-dipole transitions  $E_1$  and almost invisible in the XAS. As can be seen from Fig. 10 these transitions slightly modify the intensity of the low energy peak in the  $K$  XMCD spectrum near the edge. The intensity of quadrupole  $E_2$  transitions does not exceed 3.5% in a whole energy interval. However, in the energy region with predominantly Co  $e_g$  states at 0–3 eV above the Fermi-level,  $E_2$  transitions contribute up to 27% to the whole XMCD signal.

The experimental measurements of Co and S XAS and XMCD spectra at the  $K$  edge are highly desirable.

#### IV. SUMMARY

We have studied the electronic structure, optical properties, and x-ray magnetic circular dichroism of the  $\text{CoS}_2$  compound by means of the *ab initio* fully relativistic spin-polarized Dirac linear-muffin-tin-orbital method.

The experimental features of the optical functions are reasonably well reproduced in the LSDA calculations except for the energy shift toward higher energies of the prominent peaks in the theoretically calculated optical spectra at the 0–5 eV energy range. The disagreement with experiment might be due to a small error in the S–S bonding-antibonding splitting, and in the widths and energy position of the Co  $3d$  bands. We show that the decrease in the structure parameter  $u$  improves the energy position of the peak at around 3.5 eV in the optical reflectivity spectrum. However, the energy position of the other lower energy peaks that arises from the interband transitions between the Co  $3d$  bands does not change. One of the possible reasons is nonexact treatment of the electronic exchange and correlations. It seems quite likely that the use of a more appropriate approximation for the self-energy can give rise to a shift of the quasiparticle energy bands originated from the transition metals  $d$  states, and, as a result, give rise to a better agreement between the theory and the experiment.

Our LSDA band-structure calculations show that the  $\text{CoS}_2$  is almost a half-metallic ferromagnet with the partially filled  $e_{g\downarrow}$  subband. This result is in consistency with the point-contact Andreev reflection<sup>27</sup> and PES (Ref. 26) measurements with the observed saturation magnetic moment of  $0.85\mu_B$ ,<sup>30</sup> and with the inelastic neutron-scattering measurements.<sup>20</sup> All these experimental results indicate that the  $e_{g\downarrow}$  band in  $\text{CoS}_2$  is partially filled.

The LSDA calculations show good agreement in the shape of the Co x-ray absorption spectra at the  $L_{2,3}$  edges with the experimental measurements. They also reproduce the observed high energy shoulder at the  $L_{2,3}$  peaks situated at 5–9 eV above the edge. This feature is due to the transitions from  $2p$  core level to empty Co  $4s$  states separated from the antibonding S  $3p\sigma^*$  and Co  $e_g$  bands by the energy gap. The LSDA calculations reproduce the experimental Co  $L_{2,3}$  XMCD spectra reasonably well although the calculated magnetic dichroism is somewhat too high at the  $L_2$  edge in comparison with the experiment.

The Co  $3p_{3/2}$  and  $3p_{1/2}$  absorption spectra bands are mixed because of the small spin-orbit splitting. An intensive structure is observed in the energy region just below the absorption edge in the experimental XAS, which is not reproduced theoretically. This structure is most likely caused by the Fano effect due to an interference between the direct photoemission from the  $3d$  state and the super Coster-Kronig decay following the  $3p \rightarrow 3d$  core excitation. Such complicated processes were not considered theoretically in this study. The Co  $M_{2,3}$  XMCD spectra, besides the preedge structure, consist of two major peaks. The positive peak at around 1 eV is formed by the  $M_3$  spectrum and the higher energy negative peak at 3.5 eV is mostly due to the  $M_2$  one.

The S  $3p$ –Co  $3d$  hybridization and the spin-orbit interaction in the  $3p$  states play a crucial role for the S  $K$  edge dichroism. We found that the S  $3p$  orbital polarization originates mainly from the large spin polarization at neighboring Co atoms through the S  $3p$ –Co  $3d$  hybridization. This mechanism is different from the XMCD in transition-metal compounds in which the  $4p$  orbital polarization is induced mostly by the  $4p$  spin polarization at the atom itself through the SOI.



Due to the delocalized nature of the  $p$  states and wide extend of  $p$  wave functions,  $K$  XMCD spectra are very sensitive to the surrounding environment and, hence, the  $K$  XMCD spectroscopy can be used as an effective probe that can detect details of magnetic interatomic interactions in transition-metal compounds.

## ACKNOWLEDGMENTS

V.N.A. gratefully acknowledges the hospitality at Max-Planck-Institut für Festkörperforschung in Stuttgart during his stay there. This work was supported by Science and Technology Center in Ukraine (STCU), Project No. 4930.

- <sup>1</sup>J. A. Wilson, *Adv. Phys.* **21**, 143 (1972).
- <sup>2</sup>W. W. Kou and M. S. Seehra, *Phys. Rev. B* **18**, 7062 (1978).
- <sup>3</sup>H. S. Jarrett, W. H. Cloud, R. J. Bouchard, S. R. Butler, C. G. Frederick, and J. L. Gillson, *Phys. Rev. Lett.* **21**, 617 (1968).
- <sup>4</sup>R. L. Kautz, M. S. Dresselhaus, D. Adler, and A. Linz, *Phys. Rev. B* **6**, 2078 (1972).
- <sup>5</sup>K. Sato, *J. Phys. Soc. Jpn.* **53**, 1617 (1984).
- <sup>6</sup>Y. Nishihara, S. Ogawa, and S. Waki, *J. Phys. Soc. Jpn.* **39**, 63 (1975).
- <sup>7</sup>S. Sugano, Y. Tanabe, and H. Kamimura, *Multiplets of Transition-Metal Ions in Crystals* (Academic, New York, 1970).
- <sup>8</sup>G. Krill, P. Panissod, M. F. Lapiere, F. Gautier, C. Robert, and M. N. Eddine, *J. Phys. C* **9**, 1521 (1976).
- <sup>9</sup>F. Gautier, G. Krill, M. F. Lapiere, P. Panissod, C. Robert, G. Czjzek, J. Fink, and H. Schmidt, *Phys. Lett.* **53**, 31 (1975).
- <sup>10</sup>G. A. Prinz, *Science* **282**, 1660 (1998).
- <sup>11</sup>S. A. Wolf, D. D. Awschalom, R. A. Buhrman, J. M. Daughton, S. von Molnar, M. L. Roukes, A. Y. Chtchelkanova, and D. M. Treger, *Science* **294**, 1488 (2001).
- <sup>12</sup>G. Kirczenow, *Phys. Rev. B* **63**, 054422 (2001).
- <sup>13</sup>A. Ohsawa, Y. Yamaguchi, H. Watanabe, and H. Itoh, *J. Phys. Soc. Jpn.* **40**, 986 (1976).
- <sup>14</sup>K. Adachi, K. Sato, and M. Takeda, *J. Phys. Soc. Jpn.* **26**, 631 (1969).
- <sup>15</sup>D. W. Bullett, *J. Phys. C* **15**, 6163 (1982).
- <sup>16</sup>S. Suga, K. Inoue, M. Taniguchi, S. Shin, M. Seki, K. Sato, and T. Teranishi, *J. Phys. Soc. Jpn.* **52**, 1848 (1983).
- <sup>17</sup>G. L. Zhao, J. Callaway, and M. Hayashibara, *Phys. Rev. B* **48**, 15781 (1993).
- <sup>18</sup>H. Miyauchi, T. Koide, T. Shibara, N. Nakajima, H. Kawabe, K. Yamaguchi, A. Fujimori, H. Fukutani, K. Iio, and T. Miyadai, *J. Electron Spectrosc. Relat. Phenom.* **78**, 255 (1996).
- <sup>19</sup>T. Muro, T. Shishidou, F. Oda, T. Fukawa, H. Yamada, A. Kimura, S. Imada, S. Suga, S. Y. Park, T. Miyahara, and K. Sato, *Phys. Rev. B* **53**, 7055 (1996).
- <sup>20</sup>H. Hiraka, Y. Endoh, and K. Yamada, *J. Phys. Soc. Jpn.* **66**, 818 (1997).
- <sup>21</sup>H. Yamada, K. Terao, and M. Aoki, *J. Magn. Magn. Mater.* **177-181**, 607 (1998).
- <sup>22</sup>R. Yamamoto, A. Machida, Y. Moritomo, and A. Nakamura, *Phys. Rev. B* **59**, R7793 (1999).
- <sup>23</sup>D. Hobbs and J. Hafner, *J. Phys.: Condens. Matter* **12**, 7025 (2000).
- <sup>24</sup>S. K. Kwon, S. J. Youn, and B. I. Min, *Phys. Rev. B* **62**, 357 (2000).
- <sup>25</sup>T. Shishidou, A. J. Freeman, and R. Asahi, *Phys. Rev. B* **64**, 180401(R) (2001).
- <sup>26</sup>T. Takahashi, Y. Naitoh, T. Sato, T. Kamiyama, K. Yamada, H. Hiraka, Y. Endoh, M. Usuda, and N. Hamada, *Phys. Rev. B* **63**, 094415 (2001).
- <sup>27</sup>L. Wang, T. Y. Chen, and C. Leighton, *Phys. Rev. B* **69**, 094412 (2004).
- <sup>28</sup>P. J. Brown, K.-U. Newmann, A. Simon, F. Ueno, and R. A. Ziebeck, *J. Phys.: Condens. Matter* **17**, 1583 (2005).
- <sup>29</sup>Y. J. Jin and J. I. Lee, *Phys. Rev. B* **73**, 064405 (2006).
- <sup>30</sup>K. Adachi, M. Matsui, and M. Kawai, *J. Phys. Soc. Jpn.* **46**, 1474 (1979).
- <sup>31</sup>J. P. Perdew, K. Burke, and M. Ernzerhof, *Phys. Rev. Lett.* **77**, 3865 (1996).
- <sup>32</sup>V. Antonov, B. Harmon, and A. Yaresko, *Electronic Structure and Magneto-Optical Properties of Solids* (Kluwer, Dordrecht, 2004).
- <sup>33</sup>E. Nowack, D. Schwarzenbach, and T. Hahn, *Acta Crystallogr.* **47**, 650 (1991).
- <sup>34</sup>V. N. Antonov, B. N. Harmon, O. Andryushchenko, L. Bekenev, and A. N. Yaresko, *Low Temp. Phys.* **30**, 305 (2004).
- <sup>35</sup>V. N. Antonov, O. Jepsen, A. N. Yaresko, and A. P. Shpak, *J. Appl. Phys.* **100**, 043711 (2006).
- <sup>36</sup>O. K. Andersen, *Phys. Rev. B* **12**, 3060 (1975).
- <sup>37</sup>V. V. Nemoshkalenko, A. E. Krasovskii, V. N. Antonov, V. N. Antonov, U. Fleck, H. Wonn, and P. Ziesche, *Phys. Status Solidi B* **120**, 283 (1983).
- <sup>38</sup>J. P. Perdew and Y. Wang, *Phys. Rev. B* **45**, 13244 (1992).
- <sup>39</sup>P. E. Blöchl, O. Jepsen, and O. K. Andersen, *Phys. Rev. B* **49**, 16223 (1994).
- <sup>40</sup>R. Kubo, *J. Phys. Soc. Jpn.* **12**, 570 (1957).
- <sup>41</sup>H. S. Bennett and E. A. Stern, *Phys. Rev.* **137**, A448 (1965).
- <sup>42</sup>F. K. Richtmyer, S. W. Barnes, and E. Ramberg, *Phys. Rev.* **46**, 843 (1934).
- <sup>43</sup>F. Leuenberger, A. Parge, W. Felsch, F. Baudelet, C. Giorgetti, E. Dartyge, and F. Wilhelm, *Phys. Rev. B* **73**, 214430 (2006).
- <sup>44</sup>J. Röhrler, *J. Magn. Magn. Mater.* **47-48**, 175 (1985).
- <sup>45</sup>J. L. Campbell and T. Parr, *At. Data Nucl. Data Tables* **77**, 1 (2001).
- <sup>46</sup>D. Hobbs and J. Hafner, *J. Phys.: Condens. Matter* **11**, 8197 (1999).
- <sup>47</sup>N. Wu, Y. B. Losovyj, D. Wisbey, K. Belashchenko, M. Manno, L. Wang, C. Leighton, and P. A. Dowben, *J. Phys.: Condens. Matter* **19**, 156224 (2007).
- <sup>48</sup>F. Aryasetiawan, *Phys. Rev. B* **46**, 13051 (1992).
- <sup>49</sup>T. Muro, A. Kimura, T. Iwasaki, S. Ueda, S. Imada, T. Matsushita, A. S. T. Susaki, K. Mamiya, T. Harada, T. Kanomata, and S. Sato, *J. Electron Spectrosc. Relat. Phenom.* **88-91**, 361 (1998).
- <sup>50</sup>H. Ebert, *Rep. Prog. Phys.* **59**, 1665 (1996).
- <sup>51</sup>A. N. Yaresko, V. N. Antonov, and P. Fulde, *Phys. Rev. B* **67**, 155103 (2003).
- <sup>52</sup>M. S. S. Brooks, *Physica B (Amsterdam)* **130**, 6 (1985).

- <sup>53</sup>O. Eriksson, M. S. S. Brooks, and B. Johansson, *Phys. Rev. B* **41**, 7311 (1990).
- <sup>54</sup>L. Severin, M. S. S. Brooks, and B. Johansson, *Phys. Rev. Lett.* **71**, 3214 (1993).
- <sup>55</sup>A. Mavromaras, L. Sandratskii, and J. Kübler, *Solid State Commun.* **106**, 115 (1998).
- <sup>56</sup>A. Rogalev, J. Goulon, and C. Brouder, *J. Phys.: Condens. Matter* **11**, 1115 (1999).
- <sup>57</sup>P. G. Steeneken, Ph.D. thesis, University of Groningen, 2002.
- <sup>58</sup>F. Leuenberger, A. Parge, W. Felsch, K. Fauth, and M. Hessler, *Phys. Rev. B* **72**, 014427 (2005).
- <sup>59</sup>K. Takahashi, *Phys. Rev. B* **76**, 184422 (2007).